Super-hydrophobic coating effects on the drag of a sphere

Marco Castagna, Nicolas Mazellier, Azeddine Kourta

Super-hydrophobic coating effects on the drag of a sphere

M. CASTAGNA[a], N. MAZELLIER[b], A. KOURTA[c]

a. Univ. Orléans, INSA-CVL, PRISME, EA 4229, F45072, Orléans, France, marco.castagna@univ-orleans.fr
b. Univ. Orléans, INSA-CVL, PRISME, EA 4229, F45072, Orléans, France, nicolas.mazellier@univ-orleans.fr
c. Univ. Orléans, INSA-CVL, PRISME, EA 4229, F45072, Orléans, France, azeddine.kourta@univ-orleans.fr

Résumé :

Ce travail porte sur l'étude de l'effet des surfaces super-hydrophobes sur la traînée de sphères en chute libre dans un réservoir d'eau. Les sphères en question sont munies d'un revêtement super-hydrophobe qui prévient la pénétration du liquide dans les rugosités de surface. Il apparaît clairement que la nature de la paroi joue un rôle fondamental sur le déclenchement d'instabilités dans le sillage des sphères. Notre travail montre que le caractère super-hydrophobe favorise les oscillations transversales des sphères. Ceci se traduit par une augmentation significative de la traînée dans la gamme de nombre de Reynolds étudiée. Nos résultats mettent en avant que ce phénomène est étroitement lié â des mouvements oscillants parasites provoqués par le déplacement ample de la pellicule d'air initialement piégée dans les rugosités.

Abstract :

This work reports an experimental study of the super-hydrophobic surface effects on the free falling of spheres in water at rest. The super-hydrophobic coating prevents the penetration of the liquid in the rough surfaces. Emphasis is given to the effect of surface properties on the onset of wake instabilities. Our results evidence that the transversal motion of the falling sphere is strongly affected by the nature of the surface. Transversal oscillations are promoted by super-hydrophobic surfaces. This induces an increase of the drag in the Reynolds numbers range studied. This appears to be related to large motion of the air plastron initially entrapped in the roughness.

Key words : Friction Drag Reduction; Passive Technique; Super-hydrophobic; Transition

1 Introduction

Super-hydrophobic (SH) surfaces can be manufactured by a combination of surface roughness and chemical hydrophobicity [1]. They belong to the "biomimetics" field, that is nature inspired design [2]. In

fact, in the last decades natural examples as the lotus leaf [3][4] or the peculiar shark skin structure [5] have animated scientists toward the development of self-cleaning, anti-icing, anti-corrosion and drag reducing surfaces [6]. As far as naval and underwater applications are concerned, the SH surfaces could replace some current toxic anti-biofouling methods for hulls preservation [7], or they could be implemented as a passive technique for skin friction drag mitigation [8], as an alternative to energy consuming methods [9][10]. The physicochemical properties of SH surfaces enable indeed them to retain a gas layer (plastron) in their roughness, restricting thereby the solid/liquid contact area. Both experimental [11][12][13] and numerical studies [14][15] have proved this feature to be effective in skin friction drag reduction in external flows over flat plates and internal flows through channels. However, very few works have been dedicated to the effect of SH surfaces on bluff body wakes: numerical simulations of the flow past spheres are often limited to laminar flow conditions or require severe approximations of the complex plastron structure around the surface [16][17], whereas experimental studies focused on terminal velocity of free falling spheres in view of drag evaluation [18][19][20]. The reported results are sometimes contradictory due to the different investigated surface typologies and flow conditions. McHale et al. [18] reported drag reduction up to 15% for SH acrylic spheres coated by a spray method, for Reynolds numbers based on terminal velocity up to 3×10^4. They enhanced surface roughness by the use of micron-sized sand. Similar results were found by [19] for SH glass spheres coated by an epoxy polymer and nano-sized particles, in the same Reynolds number field. Conversely, terminal velocity reductions were found by [20] for laser-textured PTFE spheres at lower Reynolds number values (up to 5×10^3). A better understanding of the interaction between the flow and the plastron is needed to address this issue.

In this study we manufactured SH coatings by a spray method easily implementable on large scale applications. The impact of SH coatings on the drag of a free falling sphere is investigated, with emphasis on the effect of surface properties on the onset of instabilities in the path/wake. The falling spheres velocity is continuously monitored in time, and a relation between the phenomena happening at the surface and the path oscillations is proposed. In fact, it is observed on the surface of SH falling spheres the movement of macroscopic air structures with a size much larger than the SH coating roughness.

2 Experimental Set-up

The free falling sphere experiments were performed in a transparent Plexiglas® tank with 100×100 mm^2 cross-section and 650 mm height (see Fig. 1). All the tests were conducted in double-distilled water. In the experimental apparatus the spheres are released from a electromagnet placed at the water surface, in order to guarantee the sphere to be perfectly centred with respect to the tank cross-section and fully immersed into water at the beginning of the test. The temperature of the water inside the tank is monitored by a TC Direct thermocouple and was kept around 19 °C during the tests. A mirror placed at 45° with respect to the tank enables the simultaneous recording of the front and side views with a single camera. Both the recording planes are equipped with a back light to enhance contrast. Sphere motions were recorded by a Phantom V341 high-speed camera (Zeiss Makro-Planar T* 2/50 mm ZF lens), at a 2560×1100 pxl^2 resolution with a frame rate of 1000 fps. The employed recording window resulted into a conversion factor of 0.3 mm/pxl. The results reported in this paper are obtained by averaging ten different tests. A post-processing analysis of the recorded videos, carried out with the commercial software MATLAB®, allowed the reconstruction of the 3D trajectory of the falling spheres and the associated evaluation of the velocity time evolution. The uncertainties on sphere velocity were

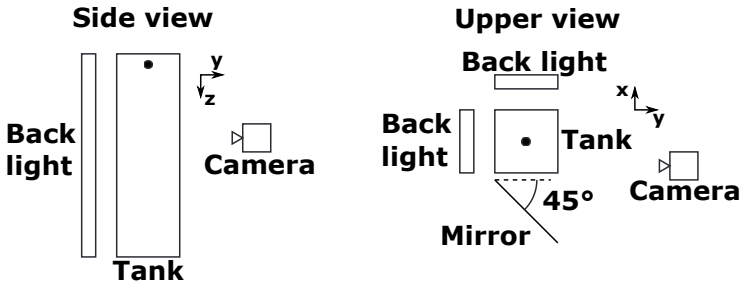

Figure 1 – Schematic of the experimental set-up for free falling sphere tests.

estimated to be lower than 5% in all cases.

Additional tests were performed in order to investigate the behaviour of the air plastron in time. In that case, a 2048×1152 pxl^2 recording window (Sigma 180 mm F2.8 APO Macro EX DG OS lens) and a 1300 fps recording speed were used. Only the front plane was recorded, and the corresponding spatial resolution was 0.06 mm/pxl.

Stainless steel spheres with nominal diameters ranging from 5 to 25 mm were used as reference (labelled NC, no coating). Three different super-hydrophobic coatings were applied over the reference steel spheres by means of a spray method. The surface of the spheres is cleaned with acetone, rinsed with water and dried. Then a primer bottom coat (Ultra-Ever Dry®) is sprayed over the surface of the spheres. The bottom coat is air dried at least for 1 hour to allow the curing process to take place. Finally, the top coat is sprayed over the sphere. The dry time is at least 2 hours in order to acquire the desired super-hydrophobic properties. The coating produced with this method will be named SH-NR (no additional roughness) hereinafter. The second super-hydrophobic coating is based on a similar manufacturing procedure with the inclusion of an intermediate layer between the bottom and the top coat. A carbon-based powder (labelled powder 220) is applied over the bottom coat before it is completely dried. A second layer of bottom coat is then sprayed over the powder with a double purpose: firmly stick the powder to the surface and provide a consistent material for the top coat to bond. For this reason the second coating will be named SH-220. The same manufacturing technique was used for the production of the third coating, whose purpose was the enhancement of the surface roughness, thanks to the use of a powder (labelled powder 80) with larger nominal particle size. Therefore, the third coating will be named SH-80. Table 1 shows major properties of the produced SH surfaces.

A METTLER TOLEDO AB104-S analytical balance with an accuracy of 0.1 mg was used for the determination of the sphere masses (m_s). The sphere diameters (d) were evaluated averaging five different measurements with an accuracy of 1 μm. The largest errors (standard deviation) on the evaluation of the sphere densities (ρ_s) are of the order of 2%. All the SH coatings determine an increase of d and m_s (up to $+10\%$ and $+5\%$ respectively), and a decrease of ρ_s (down to -20%) with respect to the corresponding reference.

	SH-NR	SH-220	SH-80
R_q [μm]	25	74	142
θ_s [°]	$160.7° \pm 1.4°$	$150.1° \pm 1.5°$	$145.7° \pm 1.0°$
θ_r [°]	$1.6° \pm 0.1°$	$2.4° \pm 0.5°$	$5.4° \pm 1.6°$

Table 1 – Major properties of the produced SH coatings. R_q, root-mean-square surface roughness; θ_s, static contact angle; θ_r, roll-off angle.

3 Results and Discussion

The reference and the SH spheres were tested in the experimental apparatus described in the previous section. Only the results concerning the 5, 8 and 10 mm diameter spheres are reported in this paper. The velocity time history was inferred from the time derivative of the trajectory.. The evaluated vertical velocity (V_Z) time evolutions are shown in Fig. 2 in the case of $d = 5$ mm. In each curve the starting time ($t_0 = 0$) is selected as the moment when the sphere effectively starts to fall after the switch-off of the electromagnet. Blank tests were performed before the experimental campaign in order to exclude significant effects of the electromagnetic field on the sphere drops. For the sake of clarity error bars are not displayed in Fig. 2. The endpoint of each curve is limited by the geometrical constraints of the experimental set-up: all the $d = 5$ mm spheres reached the respective terminal velocity. It is clear from Fig. 2 that the SH coatings determine a performance decrease with respect to the reference steel sphere in the $d = 5$ mm case: all the velocity profiles of the coated spheres lay beneath the non-coated one throughout almost the whole drop.

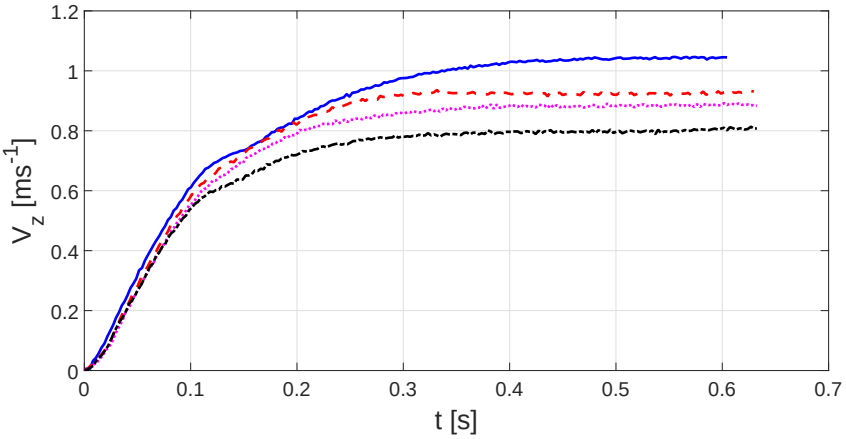

Figure 2 – Vertical velocity time evolution ($V_Z - t$) of the 5 mm diameter spheres. — (blue), stainless steel reference NC; −− (red), super-hydrophobic coating SH-NR; · · (magenta), super-hydrophobic coating SH-220; − · (black), super-hydrophobic coating SH-80.

This effect is not only due to the increase of mass and diameter and subsequent decrease of density of the sphere due to the coating application. Fig. 3 shows the experimental and theoretical V_Z profiles for the $d = 5$ mm spheres in the NC and SH-80 cases. The theoretical curve is computed by integration in time of the equation of motion proposed by Mordant and Pinton [21], where the history term has been dropped off:

$$\left(m_s + \frac{1}{2}m_f\right)\frac{dV_Z}{dt} = (m_s - m_f)\,g - \frac{1}{2}\pi\left(\frac{d}{2}\right)^2 \rho_f V_Z^2 C_D \tag{1}$$

where m_f is the mass of fluid displaced by the sphere, ρ_f the fluid density and g the gravitational acceleration. The drag coefficient (C_D) law in function of the Reynolds number (Re) is taken from [22]. As already evidenced by [21], the reference NC sphere first accelerates in a manner similar to the theoretical one, then experiences a reduction of its acceleration strongly detaching from the theoretical curve. This is due to the onset of transversal motion not taken into account by the empirical law $C_D(Re)$, which is obtained in stationary conditions.. Finally the sphere reaches its terminal velocity, in accordance with the theoretical curve. This trend is no longer followed by the SH-80 sphere: the achieved limit

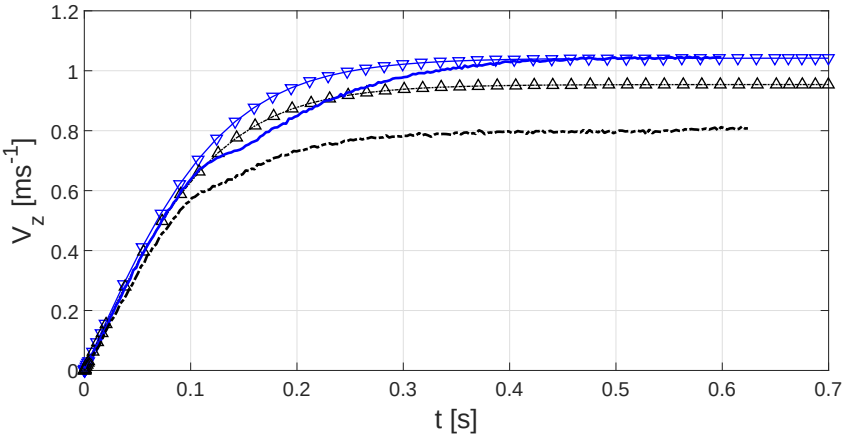

Figure 3 – Vertical velocity time evolution ($V_Z - t$) of the 5 mm diameter spheres. — (blue), stainless steel reference NC, experimental curve; $\bigtriangledown$ (blue), stainless steel reference NC, theoretical curve; $-\cdot$ (black), super-hydrophobic coating SH-80, experimental curve; $\bigtriangleup$ (black), super-hydrophobic coating SH-80, theoretical curve.

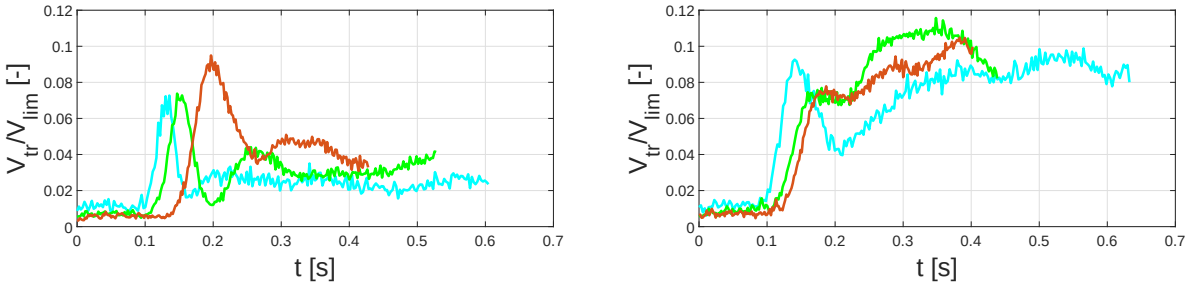

Figure 4 – Normalized transversal velocity time evolution of (a) stainless steel reference NC, (b) super-hydrophobic coating SH-80. (cyan) $d = 5$ mm, (green) $d = 8$ mm, (brown) $d = 10$ mm. The V_{tr} is normalized with respect to the limit velocity V_{lim}.

velocity is clearly lower than the value predicted by numerical computation, highlighting the fact that the $C_D(Re)$ law used for the non-coated case is not valid for SH spheres.

The identification of the transition region, that is the onset of transversal motion and path instabilities, requires the analysis of the transversal velocity $V_{tr} = \sqrt{V_X^2 + V_Y^2}$, which is shown in Fig. 4 for the NC and SH-80 cases (normalized with respect to the respective theoretical limit velocity V_{lim}). The separation between the experimental and theoretical V_Z curves highlighted in Fig. 3 is always accompanied by an abrupt peak of V_{tr}. While in the NC case larger diameters generally translate into larger V_{tr} values, this trend is partially lost for the SH-80 coating. After the peak, the V_{tr} of the reference spheres tends to strongly decrease, while in the SH-80 case it keeps to non-negligible values. Therefore SH coatings tend to promote transversal oscillations during the drop.

The effect of the transversal motion can be appreciated analysing the drag coefficient C_D evaluated in correspondence of the limit velocity (see Fig. 5). The Re is based on the limit velocity reached by each sphere and the measured diameter. As evidenced by [23], the C_D values of spheres moving rectilinearly are approximately equal to the fixed sphere case. The C_D values of the reference steel spheres NC evaluated in this study are in good agreement with the rectilinear trajectory case shown by [23]. A

drag increase was found by [23] for vibrating spheres. The transversal oscillations enhanced by the SH coatings cause the C_D values of the SH spheres to lay between the rectilinear and vibrating cases throughout the investigated Re range. The evaluated drag coefficient increment with respect to the NC spheres reaches 43%. This effect appears to be enhanced by the surface roughness: the SH-80 spheres show the highest C_D values among the SH spheres.

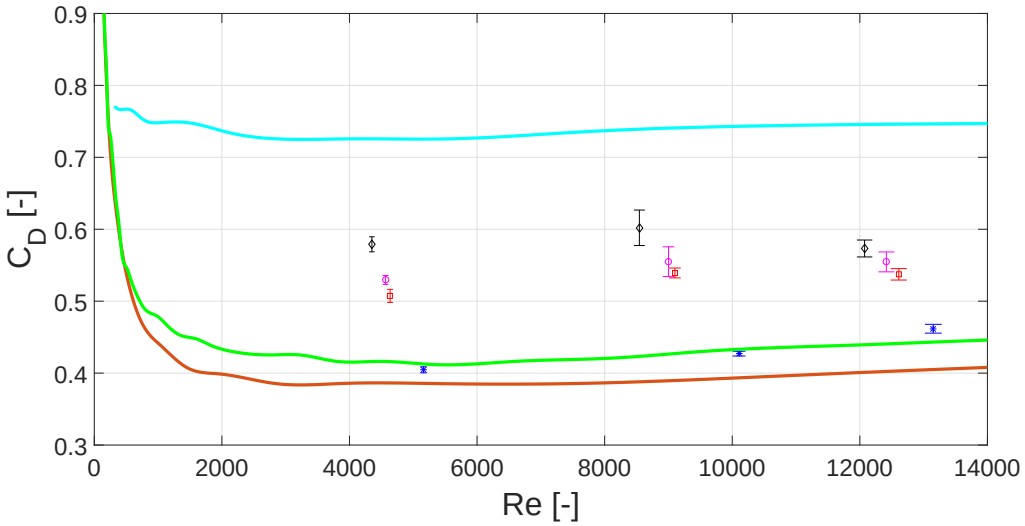

Figure 5 – Drag coefficient C_D as a function of the Reynolds number (Re) for the 5, 8, 10 mm diameter spheres. The C_D is evaluated in correspondence of the terminal velocity. $*$ (blue), stainless steel reference NC; □ (red), super-hydrophobic coating SH-NR; ○ (magenta), super-hydrophobic coating SH-220; ◇ (black), super-hydrophobic coating SH-80. — (brown) stationary sphere [23]; — (green), rectilinear trajectory spheres [23]; — (cyan), vibrating spheres [23].

These considerations are supported by an investigation of the phenomena which happen at the sphere surface during the drop. The sequence in Fig. 6, corresponding to the tank vertical height where the transition occurred for the 5 mm spheres, shows the presence of a air plastron which moves around the surface during the drop. The movement of this cushion, whose dimensions are non-negligible with respect to the sphere volume, may be related with the previous oscillation discussion. The air layer is never found in the front side of the falling sphere, probably due to the fact that it is pushed downstream by the pressure difference between the front and the rear side. The fact that the plastron nearly disappears in Fig. 6b suggests that it rotates around the backside of the falling sphere. This rotation is possibly associated with the transversal motion of the sphere.

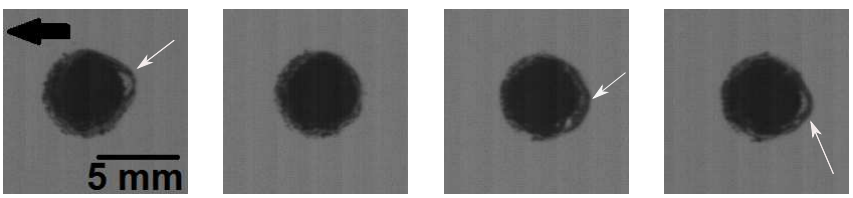

(a) $t = t_0$ (b) $t = t_0 + 45\,ms$ (c) $t = t_0 + 140\,ms$ (d) $t = t_0 + 170\,ms$

Figure 6 – Image sequence showing the movement of the air plastron (white arrows) around the rear side of a 5 mm diameter, super-hydrophobic sphere (SH-80). (a) the black arrow indicates the falling direction.

4 Conclusions

In this experimental study, SH coatings were deposited over stainless steel spheres by a spray method suitable for large scale applications. The surface roughness was enhanced by embedding micron-sized powders with different particle size. Free falling experiments were carried out to investigate the effect of the nature of the surface on the wake instabilities. It has been shown the motion of an air plastron around the rear side of SH spheres, which may induce sphere vibrations enhancement. As a result, drag increases. Our findings corroborate some results reported in literature.

Acknowledgements This work was supported by the French National Research Agency (ANR) through the *Investissements d'Avenir* program under the Labex CAPRYSSES Project (ANR-11-LABX-0006-01), and by the Direction Générale de l'Armement (DGA), Ministère de la Défense, République Française.

References

[1] N.J. Shirtcliffe, G. McHale, S. Atherton, M.I. Newton, An introduction to superhydrophobicity, Advances in Colloid and Interface Science, 161 (2010) 124–138.

[2] B. Bhushan, Y.C. Jung, Natural and biomimetic artificial surfaces for superhydrophobicity, self-cleaning, low adhesion, and drag reduction, Progress in Materials Science, 56 (2011) 1–108.

[3] W. Barthlott, C. Neinhuis, Purity of the sacred lotus, or escape from contamination in biological surfaces, Planta, 202 (1997) 1–8.

[4] J.P. Rothstein, Slip on Superhydrophobic Surfaces, Annual Review of Fluid Mechanics, 42 (2010) 89–109.

[5] B. Dean, B. Bhushan, Shark-skin surfaces for fluid-drag reduction in turbulent flow: a review, Philosophical Transactions of the Royal Society A, 368 (2010) 4775–4806.

[6] Y.-L. Zhang, H. Xia, E. Kim, H.-B. Sun, Recent developments in superhydrophobic surfaces with unique structural and functional properties, Soft Matter, 8 (2012) 11217–11231.

[7] J. Genzer, K. Efimenko, Recent developments in superhydrophobic surfaces and their relevance to marine fouling: a review, Biofouling, 22 (2006) 339–360.

[8] M.A. Samaha, H.V. Tafreshi, M. Gad-el-Hak, Superhydrophobic surfaces: from the lotus leaf to the submarine, Comptes Rendus Mecanique, 340 (2012) 18–34.

[9] K.A. Stephani, D.B. Goldstein, An examination of trapped bubbles for viscous drag reduction on submerged surfaces, Journal of Fluids Engineering, 132 (2010) 1–9.

[10] I.U. Vakarelski, J.O. Marston, D.Y.C. Chan, S.T. Thoroddsen, Drag reduction by Leidenfrost vapor layers, Physical Review Letters, 106 (2011) 1–4.

[11] E. Aljallis, M.A. Sarshar, R. Datla, V. Sikka, A. Jones, C.-H. Choi, Experimental study of skin friction drag reduction on superhydrophobic flat plates in high Reynolds number boundary layer flow, Physics of Fluids, 25 (2013) 025103-1–025103-14.

[12] C. Henoch, T.N. Krupenkin, P. Kolodner, J.A. Taylor, M.S. Hodes, A.M. Lyons, C. Peguero, K. Breuer, Turbulent drag reduction using superhydrophobic surfaces, 3rd AIAA Flow Control Conference, 5-8 June 2006, San Francisco, California, AIAA 2006-3192 1–5.

[13] R.J. Daniello, N.E. Waterhouse, J.P. Rothstein, Drag reduction in turbulent flows over superhydrophobic surfaces, Physics of Fluids, 21 (2009) 085103-1–085103-9.

[14] T. Min and J. Kim, Effects of hydrophobic surface on skin-friction drag, Physics of Fluids, 16 (2004) L55–L58.

[15] M.B. Martell, J.P. Rothstein, J.B. Perot, An analysis of superhydrophobic turbulent drag reduction mechanisms using direct numerical simulation, Physics of Fluids, 22 (2010) 065102-1–065102-13.

[16] B.R.K. Gruncell, N.D. Sandham, G. McHale, Simulations of laminar flow past a superhydrophobic sphere with drag reduction and separation delay, Physics of Fluids, 25 (2013) 043601-1–043601-16.

[17] G. McHale, M.R. Flynn, M.I. Newton, Plastron induced drag reduction and increased slip on a superhydrophobic sphere, Soft Matter, 7 (2011) 10100–10107.

[18] G. McHale, N.J. Shirtcliffe, C.R. Evans, M.I. Newton, Terminal velocity and drag reduction measurements on superhydrophobic spheres, Applied Physics Letters, 94 (2009) 064104-1–064104-3.

[19] J.-D. Brassard, D.K. Sarkar, J. Perron, Studies of drag on the nanocomposite superhydrophobic surfaces, Applied Surface Science, 324 (2015) 525–531.

[20] K.M. Tanvir Ahmmed, C. Patience, and A.-M. Kietzig, Internal and external flow over laser-textured superhydrophobic Polytetrafluoroethylene (PTFE), ACS Applied Materials & Interfaces, 8 (2016) 27411–27419.

[21] N. Mordant, J.-F. Pinton, Velocity measurement of a settling sphere, The European Physical Journal B, 18 (2000) 343–352.

[22] N.-S. Cheng, Comparison of formulas for drag coefficient and settling velocity of spherical particles, Powder Technology, 189 (2000) 395–398.

[23] M. Horowitz, C.H.K. Williamson, The effect of Reynolds number on the dynamics and wakes of freely rising and falling spheres, Journal of Fluid Mechanics, 651 (2010) 251–294.